http://dx.doi.org/10.5935/0103-5053.20130284

J. Braz. Chem. Soc., Vol. 25, No. 2, 197-207, 2014.
Printed in Brazil - ©2014 Sociedade Brasileira de Química
0103 - 5053 $6.00+0.00

Article

A New Functionalized MCM-41 Mesoporous Material for Use in Environmental Applications

José A. S. Costa,[a] Anuska C. F. S. Garcia,[a] Danilo O. Santos,[a] Victor H. V. Sarmento,[b] André L. M. Porto,[c] Maria E. de Mesquita[a] and Luciane P. C. Romão[,a]*

[a]*Departamento de Química, Universidade Federal de Sergipe, CEP 49100-000 São Cristóvão-SE, Brazil*

[b]*Departamento de Química, Universidade Federal de Sergipe, CEP 49500-000 Itabaiana-SE, Brazil*

[c]*Instituto de Química, Universidade de São Paulo, Av. Trabalhador São-Carlense, 400, CEP 13560-970 São Carlos-SP, Brazil*

Este trabalho descreve a síntese e caracterização de um novo adsorvente mesoporoso que consiste o MCM-41 funcionalizado com o ácido p-aminobenzóico modificado (PABA-Si). A síntese foi realizada pelo método hidrotermal/co-condensação. O PABA-MCM-41 foi caracterizado usando FTIR, SAXS, adsorção/desorção de N_2, MEV e TG. Os experimentos em batelada foram utilizados para determinar os efeitos da concentração inicial do adsorbato, tempo de contato e temperatura. A adsorção do benzo[a]pireno (B[a]P) alcançou o equilíbrio depois de 90 min (q_e = 27,2 μg g^{-1}) e concentrações mais altas do adsorbato foram associadas com o aumento, em ambos, da percentagem de remoção (71,0-95,7%) e no valor de q_e (20,1-27,1 μg g^{-1}). A adsorção seguiu o modelo cinético de pseudo-segunda ordem, e se ajustou ao modelo de isoterma de Langmuir. Foi verificado em temperaturas mais altas um aumento na taxa inicial de adsorção e na constante cinética. Os parâmetros termodinâmicos indicaram que o processo foi espontâneo, endotérmico e com uma tendência para desordem.

This work describes the synthesis and characterization of a new mesoporous adsorbent consisting of MCM-41 functionalized with modified p-aminobenzoic acid (PABA-Si). The synthesis was performed by a hydrothermal/co-condensation method. The PABA-MCM-41 was characterized using FTIR, SAXS, N_2 adsorption/desorption, SEM, and TG. Batch experiments were employed to determine the effects of initial adsorbate concentration, contact time, and temperature. The adsorption of benzo[a]pyrene (B[a]P) reached equilibrium after ca. 90 min (q_e = 27.2 μg g^{-1}), and higher adsorbate concentrations were associated with increases in both the percentage removal (71.0-95.7%) and the value of q_e (20.1-27.1 μg g^{-1}). The adsorption followed pseudo-second order kinetics, and was fitted using the Langmuir isotherm model. At higher temperatures, there were increases in the initial rate of adsorption and the kinetic constant. The thermodynamic parameters indicated that the process was spontaneous, endothermic, and with a tendency to disorder.

Keywords: PABA-MCM-41, adsorption, PAHs, benzo[a]pyrene, mesoporous material

Introduction

There is increasing interest in new synthetic mesoporous materials suitable for use in applications such as catalyst supports, adsorbents, optical sensors, and devices for controlled drug release. The high adsorptive capacity of these substances enables them to be used to remove toxic substances from a variety of environmental media.[1-5] The synthetic ordered mesoporous silicas of the M41S family, such as MCM-41, are especially attractive because they offer a high surface area, high adsorption capacity, a range of morphologies, and tunable mesopores.[6,7] A feature of these materials is that although they are composed of amorphous silica, they have a long-range ordered framework with uniform mesopores. The structure of hexagonal phase MCM-41 consists of the hexagonal packing of one-dimensional channels, with pore diameter of 1.5-10.0 nm and pore volume exceeding 0.3 cm^3 g^{-1}.[8]

MCM-41 can be synthesized by several methods, although the most popular is the hydrothermal technique,[9-11]

*e-mail: lucianeromao@uol.com.br

with surfactants employed in the self-assembly processes that form the mesoporous materials.[12] Modified inorganic-organic mesoporous materials can be produced by either post-grafting or in direct routes involving the co-condensation of tetraalkoxysilanes and organo-functionalized trialkoxysilanes.[13-15]

Polycyclic aromatic hydrocarbons (PAHs) are persistent pollutants that are frequently encountered in the environment. These hydrophobic organic compounds are composed of carbon and hydrogen atoms grouped into at least two condensed aromatic ring structures, and do not contain heteroatoms or substituents.[16,17] Pyrogenic and petrogenic sources are the two most important origins of anthropogenic PAHs.[18] The compounds are resistant to biodegradation and can pose long-term threats to soil and aquatic environments[19-22] since they possess toxic, carcinogenic, and/or mutagenic properties.[23-27] The United States Environmental Protection Agency (US EPA)[24] has identified 16 priority PAHs for environmental monitoring purposes. These compounds include benzo[a]pyrene (B[a]P),[28] which is also regulated by Brazilian legislation.[29,30] B[a]P is formed during the incomplete combustion of organic matter, and is found throughout the environment. The molecule consists of five fused aromatic rings, with a molecular weight of 252 g mol^{-1} and solubility in water of 0.0038 mg L^{-1}. Humans can be exposed by routes that include air, water, food, skin contact, and occupational settings.[31,32] The compound is a well-known animal carcinogen, which once absorbed is metabolically transformed into chemically active electrophiles that can form adducts with DNA.[33]

A novel co-condensation method was used to synthesize mesoporous MCM-41 functionalized with PABA, in order to obtain a material that presented a high surface area, a uniform mesopore size distribution, and good thermal stability, in which the PABA groups of the MCM-41 could interact with B[a]P. Such interaction probably occurs between the π electrons of PABA and the aromatic rings of B[a]P.[34] The material was characterized using multiple techniques, and was evaluated in terms of its ability to adsorb B[a]P.

Experimental

Standards, solvents, and reagents

A benzo[a]pyrene analytical standard (> 96% purity) was obtained from Aldrich. The solvents and reagents utilized were HPLC-grade acetonitrile, ethanol, and chloroform (all 99.9%, Tedia), cetyltrimethylammonium bromide (CTAB, 98.0%, Vetec), tetraethylorthosilicate (TEOS, 98.0%, Aldrich), 3-(triethoxysilyl)propyl isocyanate (TEPIC, Aldrich), p-aminobenzoic acid (PABA, ≥ 99.0%, Aldrich), and ammonia monohydrate ($NH_3.H_2O$, Synth), all of which were used without further purification. Ultrapure water was obtained from a Milli-Q system (Millipore Co.).

Preparation of the mesoporous MCM-41 material functionalized with PABA (PABA-MCM-41)

The modification of PABA and the hydrothermal/co-condensation synthesis of PABA-MCM-41 followed the procedure described by Li and Yan,[35] with modifications: 1.0 mmol of PABA was dissolved in 20 mL of chloroform, under agitation. 2.0 mmol TEPIC was then added to the solution drop-wise (ca. 0.50 mL), under reflux, and the mixture was heated at ca. 75.0 °C in a covered flask for approximately 12 h, under a nitrogen atmosphere. The formation of a yellow oil (here denoted PABA-Si) was observed after completion of the reaction.

The mesoporous PABA-MCM-41 was synthesized as follows: 1.1 g of CTAB was dissolved in 12 mL of concentrated $NH_3.H_2O$, followed by addition of 26 mL of deionized water and 5.5 mL of TEOS. The PABA-Si was then added to give the final molar composition: 0.12 CTAB:0.50 $NH_3.H_2O$:0.96 TEOS:0.04 PABA-Si:58.24 H_2O. The mixture was agitated at ambient temperature for 48 h, and then transferred to a Teflon flask that was closed and heated at 100 °C for 48 h in an autoclave. The solid product was separated by filtration, washed with deionized water, and air-dried at ambient temperature for 12 h. The CTAB surfactant was removed by refluxing in a solution of 1.0 mol L^{-1} CH_3CH_2OH/HCl for 48 h. The final solid product (PABA-MCM-41) was separated by filtration, washed with deionized water, and dried under vacuum at ambient temperature. The synthesis of these materials is usually performed in basic media, and NH_3 was only used to act as a catalyst. The steps of the synthesis are illustrated in Figure 1.

Characterization of the mesoporous PABA-MCM-41 material

Fourier transform infrared spectroscopy (FTIR)

The FTIR spectra were obtained in the region 4000-400 cm^{-1} using a Perkin Elmer Spectrum BX spectrophotometer, operated at ambient temperature. The samples were prepared in the form of KBr pastilles.

Small-angle X-ray scattering (SAXS)

The SAXS experiments were performed using the D2A beamline of the Brazilian Synchrotron Light Laboratory (LNLS, Campinas, Brazil), at a wavelength of 1.488 nm

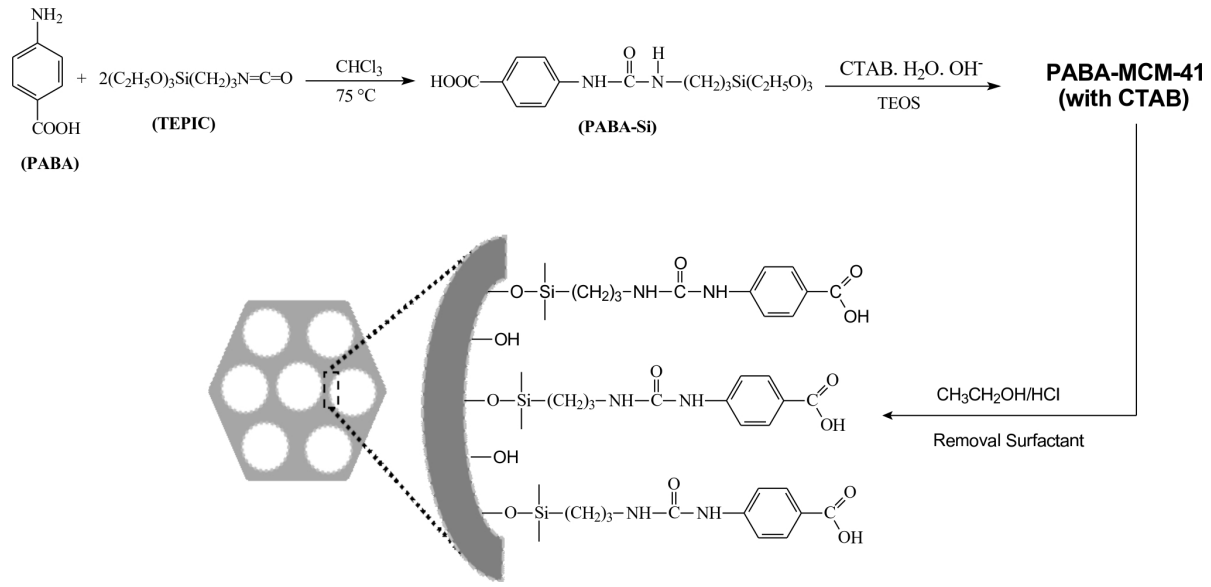

Figure 1. Synthesis procedure and proposed structure of PABA-MCM-41.

and an energy resolution (d*E*/*E*) of 0.1. The X-ray beam was conditioned by a silicon monochromator, collimated by a set of slits defining pinhole geometry, and detected by a Pilatus 300 k area detector placed 1300 mm away from the sample. The detector was offset from the main X-ray beam center to cover a scattering vector range ($q = (4\pi/\lambda)\sin\theta$; 2θ = scattering angle) from 0.5 to 5.0 nm^{-1}. The dry mesoporous powder samples were placed between two Kapton foils. All measurements were performed at room temperature. Silver behenate powder was used as a standard for calibration of the sample-to-detector distance, the detector tilt, and the direct beam position. Transmission, dark current, and Kapton foil corrections were performed on the 2D image before further data processing.

Nitrogen adsorption-desorption isotherms (BET)

Nitrogen adsorption-desorption isotherms were measured at −196.15 °C using a NOVA 1200 volumetric adsorption analyzer. Prior to the analysis, approximately 100 mg of sample was evacuated at 90 °C for 1 h in the degas port of the instrument. The Brunauer-Emmett-Teller (BET) specific surface area was calculated using adsorption data in the relative pressure range from 0.01 to 0.95. The pore volume of the sample was determined from the amount of nitrogen adsorbed at a relative pressure of about 0.95, and pore size distribution curves were calculated from analysis of the adsorption branch of the isotherm using the Barrett-Joyner-Halenda (BJH) algorithm.[36]

Scanning electron microscopy (SEM)

SEM images were obtained at a magnification of 200-5.00 K using a Leica-Zeiss Model LEO 440 microscope operated at an acceleration voltage of 20 kV, with a secondary electron detector positioned approximately 13-25 from the sample.

Thermogravimetry (TG)

TG analyses were performed under a 40 mL min^{-1} flow of nitrogen using a Shimadzu TGA-50 balance. The temperature was increased from 30 to 900 °C at a rate of 10 °C min^{-1}. Portions of sample (ca. 5.0 mg) were placed in platinum sample crucibles for the analysis.

Preparation of B[a]P standard solutions

Exactly 5.0 mg of B[a]P was dissolved in acetonitrile in a 5 mL volumetric flask. The resulting 1000 mg L^{-1} standard solution was transferred to a 250 mL volumetric flask and the volume was completed with distilled water to give a final concentration of 20 mg L^{-1} and a water/acetonitrile ratio of 98:2 (v/v). This solution was transferred to a stoppered borosilicate bottle and shaken at 300 rpm for 30 min to ensure a homogeneous distribution of the B[a]P. The PABA-MCM-41 adsorption experiments were performed after dilution of this 20 mg L^{-1} stock solution (using the same water/acetonitrile ratio).

Batch adsorption experiments

Experiments to investigate the effects of the initial B[a]P concentration, contact time, and temperature on the adsorption kinetics and isotherms were conducted individually using amber glass flasks containing 5.0 mL of B[a]P solution and 50.0 mg of PABA-MCM-41, maintained under agitation (150 rpm). All the tests were performed in duplicate. After predetermined time intervals, the samples

were allowed to rest for 5 min and then centrifuged at 3500 rpm for 2 min. The B[a]P concentrations in the supernatants were measured by HPLC (as described in Sub-Section Determination of B[a]P). A blank solution was prepared with PABA-MCM-41 in water/acetonitrile (98:2, v/v), and the control was a solution containing B[a]P alone. The removal percentages were calculated as

$$\% \text{ Removal of B[a]P} = \frac{(C_o - C_e)}{C_o} \times 100 \quad (1)$$

where C_o and C_e are the initial and final B[a]P concentrations, respectively.

Effects of initial B[a]P concentration and contact time

The influence of the initial B[a]P solution concentration was investigated using concentrations of 50, 70, 100, 150, and 200 μg L^{-1}, with a contact time of 24 h. Different contact times in the range 0-300 min were evaluated using a concentration of 200 μg L^{-1} (the concentration for which the percentage removal was greatest). The tests were performed at a temperature of 25.0 ± 0.1 °C.

Effect of temperature

The effect of temperature on adsorption of B[a]P by PABA-MCM-41 was investigated using temperatures of 25.0, 35.0, and 45.0 ± 0.1 °C, with contact times between 0 and 300 min. The thermodynamic parameters were calculated for the studied temperatures.

Kinetic study and adsorption isotherms

The experimental data were interpreted using pseudo-first order and pseudo-second order kinetic models. Once the time to equilibrium had been established, isotherms were constructed (up to 300 min), and the data obtained at temperatures of 25.0, 35.0, and 45.0 °C were fitted using the Langmuir and Freundlich isotherm models.

Determination of B[a]P

B[a]P was quantified by HPLC using a Shimadzu LC-20A Prominence instrument equipped with an LC-10AT pump, an SIL-20AT HT automatic injector, and an RF-20A fluorescence detector. Sample volumes of 20 μL were injected onto a C18 column (Vydac 201 TP 54, 250 × 4.6 mm, 5 μm) kept at a constant 30.0 °C, and the mobile phase was an isocratic flow (1.0 mL min^{-1}) of 80:20 (v/v) acetonitrile/water. The excitation and emission wavelengths used for the detection of B[a]P were 290 and 430 nm, respectively. The total analysis time was 30 min.

The external standards method was used to calculate the concentrations of B[a]P in the samples. Duplicate injections were made of B[a]P standards at concentrations ranging from 20 to 200 μg L^{-1}, and linear regression was used to generate an algorithm relating peak area to B[a]P concentration (r^2 = 0.998). A fresh calibration curve was constructed for each sequence of analyses.

Results and Discussion

Mesoporous MCM-41 functionalized with PABA

Fourier transform infrared spectroscopy

FTIR was used to confirm the presence of the organic PABA ligand covalently bonded with MCM-41. The spectra for the PABA, PABA-Si, and PABA-MCM-41 material are illustrated in Figure 2. The spectrum for PABA-Si (Figure 2b) included absorption bands at 1199 cm^{-1} (C–Si stretching) and at 1110 and 1042 cm^{-1} (Si–O stretching), which are characteristic of the triethoxylsilane functional group.[37] The insertion of TEPIC into PABA was confirmed by the presence of a band at 1682 cm^{-1} corresponding to the absorption of amide groups (–CONH–), and bands centered at 2934 and 2882 cm^{-1} corresponded to vibration of the methylene group (–$(CH_2)_3$–) of TEPIC.[35] A band at 1554 cm^{-1} (δNH vibration) provided further evidence of the formation of amide groups.[35,38]

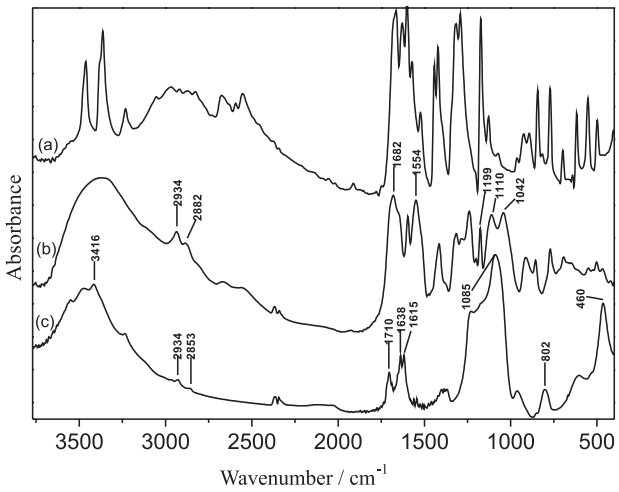

Figure 2. FTIR spectra of (a) PABA, (b) PABA-Si, and (c) PABA-MCM-41.

A broad absorption band at 3416 cm^{-1} corresponded to O–H stretching of adsorbed water molecules and the silanol groups (Si–OH) (Figure 2c).[39,40] Formation of the Si–O–Si framework was confirmed by the bands located at 1085 cm^{-1} (ν_{as}, Si–O), 802 cm^{-1} (ν_s, Si–O), and 460 cm^{-1} (δ, Si–O–Si).[35,41] In addition, the bands corresponding to amide –CONH– vibration (at 1638 and 1615 cm^{-1}), stretching of carboxylic acid C=O (at 1710 cm^{-1}), and methylene group

vibrations (at 2934 and 2853 cm^{-1}), which are related to PABA-Si,[35] were also observed for PABA-MCM-41. This is consistent with the PABA group in the framework remaining intact after the hydrolysis-condensation reaction and the surfactant extraction procedure.[13] The bands at 1554 and 1400 cm^{-1} correspond to PABA-Si (Figure 2b), and were not detectable in the case of PABA-MCM-41 (Figure 2c). It is possible that not all the PABA-Si added to the reaction medium was incorporated in the pores of PABA-MCM-41. Elimination of CTAB from the structure of the mesoporous PABA-MCM-41 was confirmed by the absence of intense bands at 2921 and 2851 cm^{-1} related to stretching of the C–H bond of CTAB (Figure 2c), as well as absence of the band related to deformation of the C–H bond of CTAB at 1400 cm^{-1}.[40]

Small-angle X-ray scattering (SAXS)

SAXS measurements can help to characterize mesoporous substances and nanostructured host/guest hybrid materials. The SAXS pattern for PABA-MCM-41 (Figure 3) revealed three intense peaks, q_{100}, q_{110}, and q_{200}, related to the (1 0 0), (1 1 0), and (2 0 0) diffraction planes, respectively. The type of mesostructure can be identified by analysis of the relative peak distance ratios (q_{100}/q_{100}, q_{110}/q_{100} and q_{200}/q_{100}). The three intense peaks, whose positions are in a q_{hk}/q_{100} ratio of 1:√3:2 (*h, k* and *l* are the Miller Indices), correspond, respectively, to the (1 0 0), (1 1 0) and (2 0 0) diffraction planes of the hexagonal (P6mm) mesophases formed by the compact packing of cylindrical tubes. The SAXS curves (Figure 3) are indicative of the hexagonal mesostructure that is typical of the M41S family, confirming the synthesis of PABA-MCM-41. Furthermore, the position of the first peak, q_{100}, allows direct determination of the center-center distance between adjacent tubes using $a_0 = (2/\sqrt{3})d$, where $d = 2\pi/q_{100}$.[42, 43] The calculated d and a_o values are given in Table 1.

Nitrogen adsorption-desorption isotherms

The N_2 adsorption-desorption isotherms for PABA-MCM-41 are shown in Figure 4, together with the pore size distributions (Figure 4 inset). According to the IUPAC classification, type IV isotherms and type H1 hysteresis loops at low relative pressure are characteristic

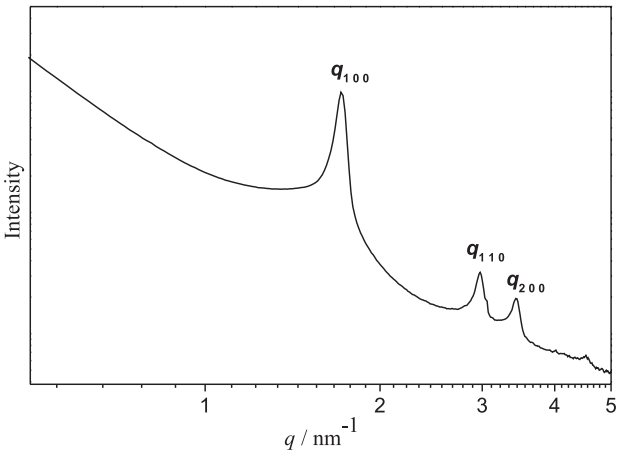

Figure 3. X-ray scattering intensity for PABA-MCM-41.

of mesoporous MCM-41 materials with uniform size distributions.[44-47] This was confirmed by narrow pore size distributions that possessed a single peak. The presence of a hysteresis loop, indicating capillary condensation,[45] at relative pressure (P/P_0) > 0.39 was indicative of the presence of a well-defined array of regular mesopores, which is important for efficient adsorption. The specific surface area and the pore size were calculated using the Brunauer-Emmett-Teller (BET) and Barrett-Joyner-Halenda (BJH) methods, respectively. The textural and structural properties of PABA-MCM-41 (BET surface area, pore volume, and pore size) are summarized in Table 1.

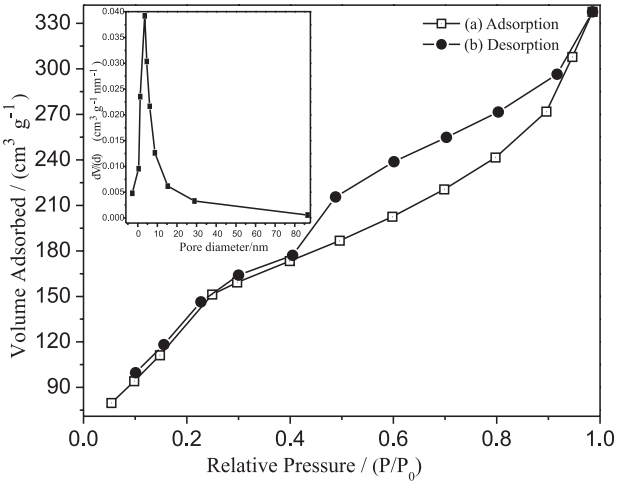

Figure 4. Nitrogen (a) adsorption and (b) desorption isotherms for PABA-MCM-41. Inset: pore size distribution.

Table 1. Textural and structural properties of PABA-MCM-41

Sample	d_{100} / nm	S_{BET} / (m^2 g^{-1})	V / (cm^3 g^{-1})	D_{BJH} / nm	a_0 / nm	W_t / nm
PABA-MCM-41	3.6	556.4	0.33	3.6	4.2	0.61

d_{100}: d(100) spacing; a_0: center-center distance ($a_0 = (2/\sqrt{3})d$; S_{BET}: BET surface area; V: pore volume; D_{BJH}: pore diameter; W_t: wall thickness, calculated as $a_0 - D_{BJH}$.

Scanning electron microscopy

SEM was used to determine the morphology of the synthesized particles. The SEM image obtained for PABA-MCM-41 (Figure 5) showed the presence of agglomerated spherical particles, which are a typical feature of mesoporous materials.[48]

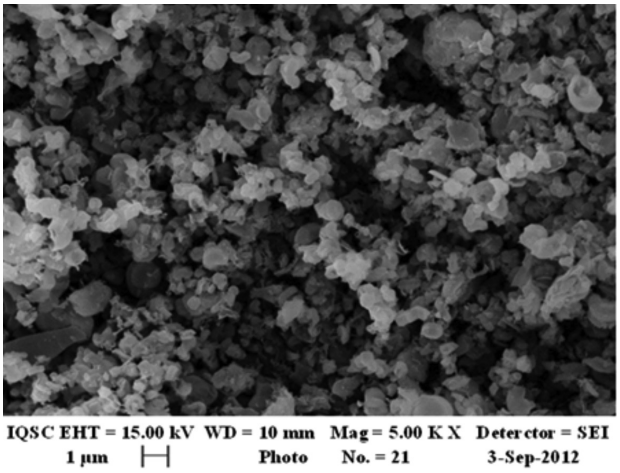

Figure 5. Scanning electron micrograph of PABA-MCM-41.

Thermogravimetry (TG)

The TG curve obtained for PABA-MCM-41 after removal of the CTAB surfactant (Figure 6) was typical of mesoporous materials based on MCM-41.[10] There were three main processes of mass loss. At 30-185 °C, water and residual solvents physically adsorbed on the mesoporous material were eliminated without any breaking of chemical bonds.[49] Decomposition of the organic matter of PABA occurred at 185-379 °C, and at 379-750 °C there was combustion of the residual organic matter of PABA as well as condensation of adjacent silanol groups resulting from linking of the siloxanes situated within the pores of the mesoporous material.[41,50-52]

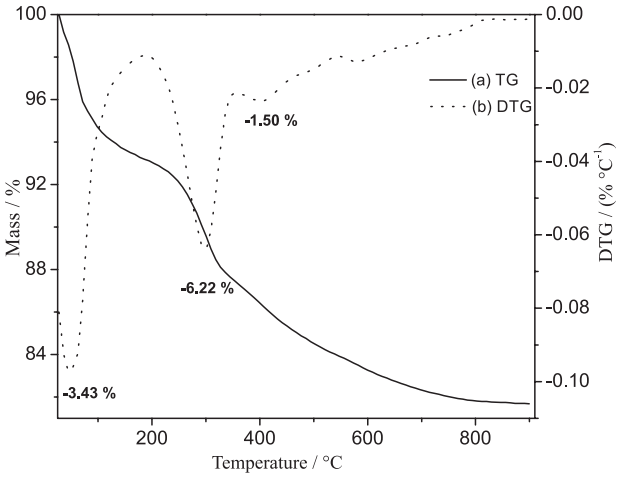

Figure 6. (a) TG and (b) DTG curves for PABA-MCM-41 after removal of CTAB, using a nitrogen atmosphere and a heating rate of 10 °C min^{-1}.

Since the last two events were related to the decomposition and combustion, respectively, of the organic matter derived from the PABA, the mass loss (of approximately 7.72%) reflected the percentage of PABA in the mesoporous material. These observations suggest that PABA-MCM-41 is thermally stable below 185 °C; this is an important finding since it indicates that PABA-MCM-41 could be used as an adsorbent in high-temperature applications.

Batch adsorption experiments

Effects of initial concentration and contact time

The influence of the initial B[a]P concentration was studied in the range 50-200 µg L^{-1}. The percentage removal showed a clear dependence on the initial amount of B[a]P in the solution (Figure 7), with values of 71.0, 78.6, 84.3, 89.4, and 95.7% obtained for concentrations of 50, 70, 100, 150, and 200 µg L^{-1}, respectively. The corresponding quantities of B[a]P adsorbed at equilibrium (q_e) were 20.1, 22.3, 25.3, and 27.1 µg g^{-1}, respectively. This behavior could be explained by adsorption occurring mainly at the outermost sites of the PABA-MCM-41 surface when the initial adsorbate concentration was low, with migration towards sites deeper within the mesoporous material at higher initial adsorbate concentrations.[53] The high adsorption capacity reflects the satisfactory textural and structural properties of the adsorbent (Table 1).

The effect of contact time on B[a]P adsorption was studied using an initial concentration of 200 µg L^{-1} (for which the greatest percentage removal was achieved). There was an initial rapid increase in adsorption capacity (Figure 7b), and attainment of equilibrium after approximately 90 min, with 96.2% removal and a q_e value of 27.2 µg g^{-1}. The adsorption kinetics of PABA-MCM-41 could therefore be characterized as being relatively fast.

Gong *et al.*[54] used activated carbon to adsorb PAHs and achieved an average B[a]P removal of 85.0%. Costa *et al.*[34] reported B[a]P removal values of 91.5, 43.8, and 37.2% using the zeolite materials HBEA, HZSM-5, and HUSY as adsorbents. Zeledón-Toruño *et al.*[55] obtained a B[a]P removal efficiency of 82.0% using an immature coal (leonardite).

Effect of temperature and the kinetics of adsorption

Temperature is one of the most important factors influencing adsorption systems, since it affects the rates of many processes. According to Robinson *et al.*,[56] and Ho and Mckay,[57] the kinetic energy and mobility of the adsorbate increase at higher temperatures. This could increase the

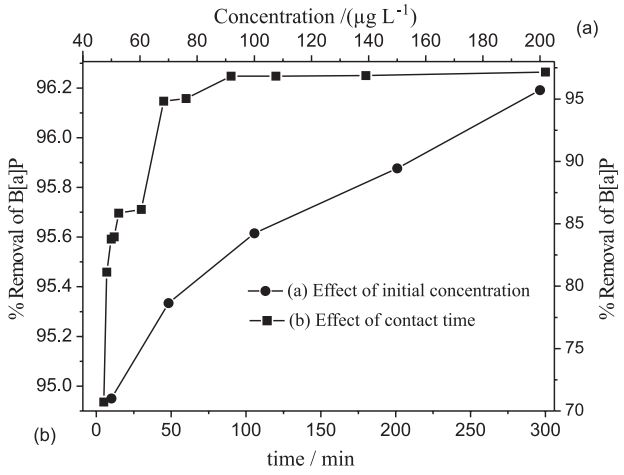

Figure 7. (a) Effect of initial concentration on adsorption of benzo[a] pyrene. Conditions: 50.0 mg of PABA-MCM-41, 5.0 mL of B[a]P solution (at concentrations of 50, 70, 100, 150, and 200 μg L^{-1}), 24 h contact time, and agitation at 150 rpm. (b) Effect of contact time on adsorption of B[a]P. Conditions: Initial B[a]P concentration of 200 μg L^{-1}, 50.0 mg of PABA-MCM-41, temperature of 25.0 ± 0.1 °C, agitation at 150 rpm, and contact time of 300 min.

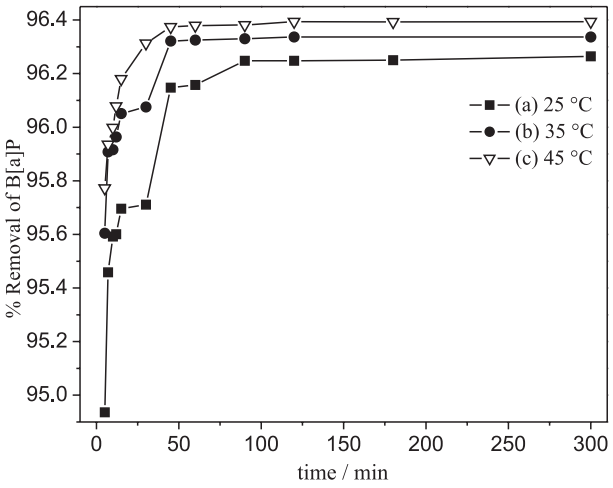

Figure 8. Effect of temperature on adsorption of benzo[a]pyrene. Conditions: Initial B[a]P concentration of 200 μg L^{-1}, 50.0 mg of PABA-MCM-41, temperatures of (a) 25.0, (b) 35.0, and (c) 45.0 °C, agitation at 150 rpm, and contact time of 300 min.

rate of intra-particle diffusion of B[a]P to the pores of PABA-MCM-41, and therefore also affect the solubility and chemical potential of the compound.[58]

The effect of temperature is reflected in the adsorption rate constant. Experiments performed at three or more different temperatures can be used to obtain the corresponding rate constants, which then enable calculation of the activation energy of the process using the Arrhenius equation,[59,60]

$$\ln k_{ads} = \ln A - \frac{E_a}{RT}, \quad (2)$$

where k_{ads} is the first or second order adsorption rate constant, A (s^{-1}) is the Arrhenius frequency factor, E_a (kJ mol^{-1}) is the activation energy of the adsorption process, R is the gas constant (8.314 J mol^{-1} K^{-1}), and T (K) is the absolute temperature.

Plotting $\ln k_{ads}$ against $1/T$ produces a linear relationship with an angular coefficient of $-E_a/R$, from which the activation energy can be calculated. The Arrhenius frequency factor (A) is obtained from the linear coefficient ($\ln A$). The effect of temperature was investigated at 25.0, 35.0, and 45.0 °C (Figure 8). No significant differences were observed for either the percentage removal (96.2, 96.3, and 96.4%, respectively) or the quantities of B[a]P adsorbed (q_e) (27.2, 27.3, and 27.4 μg g^{-1}, respectively). An advantage of this material is therefore that it can be employed at ambient temperature, hence reducing the energy costs of processes used to remove environmental pollutants.

Knowledge of the adsorption kinetics is important for an understanding of the mechanism and efficiency of a process. Both pseudo-first order and pseudo-second order kinetic models have been used for this purpose.[61] The pseudo-first order equation may be written in the form

$$\frac{dq_t}{dt} = k_1(q_e - q_t) \quad (3)$$

where q_t and q_e are the amounts of B[a]P (μg g^{-1}) adsorbed at time t and at equilibrium, respectively, and k_1 (min^{-1}) is the equilibrium rate constant for pseudo-first order sorption. Integrating equation (3) by applying the boundary condition $q_t = 0$ at $t = 0$ results in

$$\ln(q_e - q_t) = \ln q_e - k_1 t \quad (4)$$

The slopes and intercepts of plots of $\ln (q_e - q_t)$ against t were used to determine the first order rate constant ($-k_1$) and the adsorption at equilibrium ($\ln q_e$).

The pseudo-second order equation may be expressed as

$$\frac{dq_t}{dt} = k_2(q_e - q_t)^2 \quad (5)$$

where k_2 (g μg^{-1} min^{-1}) is the equilibrium rate constant for pseudo-second order sorption. Considering the boundary condition ($q_t = 0$ at $t = 0$), the integrated form of equation (5) is

$$q_t = \frac{tq_e^2 k_2}{1 + tq_e k_2} \quad (6)$$

The pseudo-second order kinetic model can be linearized in four different ways, although the most popular (used here) is

$$\frac{t}{q_t} = \frac{1}{k_2 q_e^2} + \frac{t}{q_e} \quad (7)$$

The equilibrium adsorption capacity ($q_{e(\mathrm{calc})}$) and the second order rate constant (k_2) can be determined experimentally from the slope and intercept of a plot of t/q_t against t. For this model, the initial adsorption rate is described by

$$h_i = k_2 q_e^2 \tag{8}$$

and the half-life can be calculated using

$$t_{1/2} = \frac{1}{q_e k_2}, \tag{9}$$

where h_i (μg g^{-1} min^{-1}) is the initial adsorption rate and $t_{1/2}$ (min) is the half-life.[44,62,63]

The results obtained from the linearized models for adsorption of B[a]P on PABA-MCM-41 at the three different temperatures are listed in Table 2, together with the values of the pseudo-first order and pseudo-second order equation parameters and the correlation coefficients.

The pseudo-second order kinetic model provided the best fit to the experimental data. Linear correlation coefficients (r^2) of 1.000 were obtained for all the temperatures studied, and the calculated values of q_e were very close to the experimental values ($q_{e\,(exp.)}$). At the higher temperatures, the values of k_2 and the initial adsorption rate (h_i) increased, resulting in lower $t_{1/2}$ values, and there was a small increase in the quantity adsorbed (q_e).

Using equation (2) and the pseudo-second order rate constants obtained at different temperatures, values of 20.79×10^6 s^{-1} and 43.63 kJ mol^{-1} were calculated for the Arrhenius frequency factor (A) and activation energy (E_a), respectively. Values of E_a in the range 5-40 kJ mol^{-1} are characteristic of physical adsorption processes, while values of 40-80 kJ mol^{-1} are indicative of chemisorption.[60,61]

Adsorption isotherms

Adsorption data are often described using adsorption isotherms, such as those of Freundlich or Langmuir. These isotherms relate the amount of solute adsorbed at equilibrium per weight of adsorbent, q_e (μg g^{-1}), to the adsorbate concentration at equilibrium, C_e (μg L^{-1}). The Freundlich isotherm is the most widely used non-linear sorption model and is not restricted to the formation of the monolayer, with a heterogeneous active site energy distribution and interactions between adsorbed molecules.[7,64-66] The general form of this model is given by

$$q_e = k_F C_e^{1/n} \tag{10}$$

where k_F is the adsorption capacity and n is the adsorption intensity.

The logarithmic form of Equation (10) is

$$\ln q_e = \ln k_F + \frac{1}{n} \ln C_e \tag{11}$$

where k_F and $1/n$ can be determined from a linear plot of $\ln q_e$ against $\ln C_e$.

The Langmuir model represents one of the first theoretical treatments of nonlinear sorption and proposes that uptake occurs on a homogeneous surface by monolayer sorption without interaction between adsorbed molecules. In addition, the model assumes uniform surface adsorption energy and no transmigration of the adsorbate.[14,64,67]

The Langmuir isotherm is given by

$$q_e = \frac{Q_{\max} b C_e}{1 + b C_e} \tag{12}$$

where Q_{max} (μg g^{-1}) and b (L μg^{-1}) are Langmuir constants related to the adsorption capacity and the energy of adsorption, respectively. Equation 12 is usually linearized to obtain

$$\frac{C_e}{q_e} = \frac{1}{b Q_{\max}} + \frac{C_e}{Q_{\max}} \tag{13}$$

The values of k_F, $1/n$, Q_{max}, b, and the linear regression correlation coefficients for the Freundlich (r^2_F) and Langmuir (r^2_L) models are given in Table 3. The correlation coefficients for the fits were $0.832 < r^2_F < 0.930$ and

Table 2. Comparison of the pseudo-first order and pseudo-second order kinetic models for the adsorption of benzo[a]pyrene on the mesoporous material PABA-MCM-41

T / °C	$q_{e\,(exp.)}$ / (μg g^{-1})	Pseudo-first order			Pseudo-second order				
		$q_{e\,(calc.)}$ / (μg g^{-1})	k_1 / min^{-1}	r^2	$q_{e\,(calc.)}$ / (μg g^{-1})	k_2 / (g μg^{-1} min^{-1})	h_i / (μg g^{-1} min^{-1})	$t_{1/2}$ / min	r^2
25.0	27.2	0.29	0.03	0.828	27.2	0.44	324.7	0.08	1.000
35.0	27.3	0.27	0.07	0.940	27.3	0.95	709.2	0.04	1.000
45.0	27.4	0.11	0.04	0.883	27.4	1.32	980.4	0.03	1.000

T: temperature; $q_{e(exp)}$ and $q_{e(calc)}$: quantities of B[a]P adsorbed at equilibrium, obtained experimentally and calculated, respectively; k_1 and k_2: pseudo-first order and pseudo-second order rate constants, respectively; r^2: linear correlation coefficient; h_i: initial adsorption rate; $t_{1/2}$: half-life.

Table 3. Model parameters for the adsorption of benzo[a]pyrene on PABA-MCM-41 at different temperatures

T / °C	Freundlich			Langmuir		
	k_F / (μg g^{-1})	*1/n*	r^2_F	Q_{max} / (μg g^{-1})	b / (L μg^{-1})	r^2_L
25.0	40.2	0.039	0.930	27.8	2.69	0.980
35.0	44.2	0.038	0.900	27.9	3.60	0.999
45.0	44.1	0.040	0.832	28.0	4.57	0.990

T: temperature; k_F: adsorption capacity; n: adsorption intensity; r^2: correlation coefficient; Q_{max} and b: Langmuir constants.

Table 4. Thermodynamic parameters for the adsorption of benzo[a]pyrene on PABA-MCM-41 at different temperatures

T / °C	K_c / (L g^{-1})	ΔG / (kJ mol^{-1})	ΔH / (kJ mol^{-1})	ΔS / (J mol^{-1} K^{-1})	r^2
25.0	2.57	–2.35			
35.0	2.63	–2.48	1.45	12.73	0.996
45.0	2.67	–2.59			

T: temperature; K_c: equilibrium constant; ΔG: Gibbs free energy; ΔH: enthalpy; ΔS: entropy.

$0.980 < r^2_L < 0.999$ for the Freundlich and Langmuir equations, respectively, indicating that the Langmuir model provided the best description of the adsorption of B[a]P on PABA-MCM-41, especially at lower temperatures. The values obtained using the Langmuir model showed an increase of maximum B[a]P adsorption capacity (Q_{max}), from 27.8 to 28.0 μg g^{-1}, when the temperature was increased from 25.0 to 45.0 °C. This is consistent with the generally accepted description of MCM-41, which considers the adsorption sites to be homogeneously distributed[1,44,68] and to possess equal adsorption energies.[55,69,70]

Thermodynamic parameters

The following equations were used to determine changes in the Gibbs free energy (ΔG), enthalpy (ΔH), and entropy (ΔS):

$$K_C = \frac{q_e}{C_e} \quad (14)$$

$$\Delta G = -RT \ln K_C \quad (15)$$

$$\ln K_C = \frac{\Delta S}{R} - \frac{\Delta H}{RT} \quad (16)$$

In the above equations, K_c (L g^{-1}) is the equilibrium constant, q_e (μg g^{-1}) is the amount of solute adsorbed on the adsorbent at equilibrium, C_e (μg L^{-1}) is the equilibrium concentration of the solute in solution, T is the temperature in Kelvin, and R (J mol^{-1} K^{-1}) is the gas constant.[64,67,71] ΔH and ΔS were obtained from the slope and intercept of Van't Hoff plots of ln K_c against 1/T.

The calculated values of the thermodynamic parameters for the adsorption of B[a]P on PABA-MCM-41 at different temperatures are provided in Table 4. The negative values of ΔG for the temperatures used are indicative of the spontaneous nature of the adsorption process. The decrease in ΔG with increase in temperature shows that the adsorption was favored at higher temperatures. The positive value of ΔS suggests that there was an increase of randomness at the solid/solution interface during the adsorption process, while the positive value of ΔH indicates that the adsorption was endothermic.

Conclusions

A hydrothermal/co-condensation method was successfully used to synthesize a mesoporous material functionalized with the p-aminobenzoic acid ligand modified with 3-(triethoxysilyl)-propyl isocyanate. Mesoporous PABA-MCM-41 possessed the hexagonal mesostructure typical of the M41S family, with a high surface area, a uniform mesopore size distribution, and good thermal stability. The material presented a type IV isotherm and type H1 hysteresis. The adsorption of B[a]P by PABA-MCM-41 was rapid, reaching equilibrium after around 90 min, and the removal percentage increased at higher adsorbate concentrations. The adsorption kinetics followed the linearized pseudo-second order model, and the best isotherm fit was achieved using the Langmuir model. Both the kinetic constant for the adsorption and the initial adsorption rate increased at higher temperatures. The calculated thermodynamic parameters were indicative of an endothermic process that was spontaneous in nature, with a tendency towards disorder. The results demonstrated the suitability of PABA-MCM-41 as an adsorbent material for the removal of polycyclic aromatic compounds present in surface waters and effluents.

Acknowledgments

The authors thank CNPq (Conselho Nacional de Desenvolvimento Científico e Tecnológico) for research grants (Processes 309342/2010-4 and 135602/2011-4), and LNLS for the SAXS measurements (Project SAXS1 12642).

References

1. Qin, Q.; Ma, J.; Liu, K.; *J. Hazard. Mater.* **2009**, *162*, 133.
2. Vidal, C. B.; Barros, A. L.; Moura, C. P.; Lima, A. C. A.; Dias, F. S.; Vasconcellos, L. C. G.; Fechine, P. B. A.; Nascimento, R. F.; *J. Colloid Interface Sci.* **2011**, *357*, 466.
3. Yang, X.; Guan, Q.; Li, W.; *J. Environ. Manage*. **2011**, *92*, 2939.
4. Kamarudin, K. S. N.; Alias, N.; *Fuel Process. Technol.* **2013**, *106*, 332.
5. Zhou, Y.; Tao, Y. F.; Yang, J.; Lin, W. G.; Wan, M. M.; Wang, Y.; Zhu, J. H.; *J. Hazard. Mater*. **2011**, *190*, 87.
6. Xiao, N.; Wang, L.; Liu, S.; Zou, Y.; Wang, C.; Ji, Y.; Song, J.; Li, F.; Meng, X.; Xiao, F.-S.; *J. Mater. Chem*. **2009**, *19*, 661.
7. Mangrulkar, P. A.; Kamble, S. P.; Meshram, J.; Rayalu, S. S.; *J. Hazard. Mater*. **2008**, *160*, 414.
8. Binnemans, K.; *Chem. Rev*. **2009**, *109*, 4283.
9. Meynen, V.; Cool, P.; Vansant, E. F.; *Microporous Mesoporous Mater*. **2009**, *125*, 170.
10. Melo, R. A. A.; Giotto, M. V.; Rocha, J.; Urquieta-González, E. A.; *Mater. Res*. **1999**, *2*, 173.
11. Sangchoom, W.; Mokaya, R.; *J. Mater. Chem*. **2012**, *22*, 18872.
12. Corma, A.; Kan, Q.; Navarro, M. T.; Pérez-Pariente, J.; Rey, F.; *Chem. Mater*. **1997**, *9*, 2123.
13. Li, H. R.; Lin, J.; Fu, L. S.; Guo, J. F.; Meng, Q. G.; Liu, F. Y.; Zhang, H. J.; *Microporous Mesoporous Mater*. **2002**, *55*, 103.
14. Anbia, M.; Mohammadi, N.; Mohammadi, K.; *J. Hazard. Mater*. **2010**, *176*, 965.
15. Cao, Q.-Y.; Chen, Y.-H.; Liu, J.-H.; Gao, X.-C.; *Inorg. Chem. Commun*. **2009**, *12*, 48.
16. Li, C.-H.; Yea, C.; Wong, Y.-S.; Tam, N. F.-Y.; *J. Hazard. Mater*. **2011**, *190*, 786.
17. Chen, J.; Wong, M.-H.; Wong, Y.-S.; Tam, N. F.-Y.; *Mar. Pollut. Bull*. **2008**, *57*, 695.
18. Liu, Y.; Chen, L.; Huang, Q.-H.; Li, W.-Y.; Tang, Y.-J.; Zhao, J.-F.; *Sci. Total Environ*. **2009**, *407*, 2931.
19. Zhang, Y.; Wang, F.; Yang, X.; Gu, C.; Kengara, F. O.; Hong, Q.; Lv, Z.; Jiang, X.; *Appl. Microbiol. Biotechnol*. **2011**, *90*, 1063.
20. Clemente, A. R.; Anazawa, T. A.; Durrant, L. R.; *Braz. J. Microbiol*. **2001**, *32*, 255.
21. Arulazhagan, P.; Vasudevan, N.; *Mar. Pollut. Bull*. **2011**, *62*, 388.
22. Wang, C.; Wang, F.; Wang, T.; Bian, Y.; Yang, X.; Jiang, X.; *J. Hazard. Mater*. **2010**, *176*, 41.
23. Li, C.-H.; Wong, Y.-S.; Tam, N. F.-Y.; *Bioresour. Technol*. **2010**, *101*, 8083.
24. US Environmental Protection Agency (US EPA); *Provisional Guidance for Quantitative Risk Assessment of Polycyclic Aromatic Hydrocarbons*; Office of Research and Development, Office of Health and Environmental Assessment: Washington D. C., EPA/600/R-93/089, 1993.
25. Chen, J. L.; Wong, M. H.; Wong, Y. S.; Tam, N. F.-Y.; *J. Hazard. Mater.* **2011**, *190*, 409.
26. Chupungars, K.; Rerngsamran, P.; Thaniyavarn, S.; *Int. Biodeterior. Biodegrad*. **2009**, *63*, 93.
27. Janbandhu, A.; Fulekar, M. H.; *J. Hazard. Mater*. **2011**, *187*, 333.
28. Keum, Y.-S.; Seo, J.-S.; Hu, Y.; Li, Q. X.; *Appl. Microbiol. Biotechnol*. **2006**, *71*, 935.
29. Leis Brasil, Conselho Nacional do Meio Ambiente, Resolução Conama No. 357, de 17 de março de 2005, DOU 18.03.2005.
30. Leis Brasil, Ministério da Saúde, Portaria MS No. 2914 de 12/12/2011, DOU: 14/12/2011.
31. Simarro, R.; González, N.; Bautista, L. F.; Sanz, R.; Molina, M. C.; *Water, Air, Soil Pollut*. **2011**, *217*, 365.
32. Jules, G. E.; Pratap, S.; Ramesh, A.; Hooda, D. B.; *Toxicol*. **2012**, *295*, 56.
33. Elie, M. R.; Clausen, C. A.; Geiger, C. L.; *J. Hazard. Mater*. **2012**, *203-204*, 77.
34. Costa, A. A.; Wilson, W. B.; Wang, H.; Campiglia, A. D.; Dias, J. A.; Dias, S. C. L.; *Microporous Mesoporous Mater.* **2012**, *149*, 186.
35. Li, Y.; Yan, B.; *Microporous Mesoporous Mater*. **2010**, *128*, 62.
36. Wan, M. M.; Yang, J. Y.; Qiu, Y.; Zhou, Y.; Guan, C. X.; Hou, Q.; Lin, W. G.; Zhu, J. H.; *ACS Appl. Mater. Interfaces* **2012**, *4*, 4113.
37. Qiao, X.-F.; Yan, B.; *Eur. Polym. J*. **2009**, *45*, 2002.
38. Kong, L.-L.; Yan, B.; Li, Y.; *J. Alloys Compounds* **2009**, *481*, 549.
39. Rana, S.; Mallick, S.; Mohapatra, L.; Varadwaj, G. B. B.; Parida, K. M.; *Catal. Today* **2012**, *198*, 52.
40. Oliveira, A. C.; Rangel, M. C.; Fierro, J. L. G.; Reyes, P.; Oportus, M.; *Quim. Nova* **2005**, *28*, 37.
41. Braga, R. M.; Barros, J. M. F.; Melo, D. M. A.; Melo, M. A. F.; Aquino, F. M.; Freitas, J. C. O.; Santiago, R. C.; *J. Therm. Anal. Calorim*. **2013**, *111*, 1013.
42. Wang, H.; Ma, Y.; Tian, H.; Tang, N.; Liu, W.; Wang, Q.; Tang, Y.; *Dalton Trans*. **2010**, *39*, 7485.
43. Freitas, F. G.; Sarmento, V. H. V.; Santilli, C. V.; Pulcinelli, S. H.; *Colloids Surf. A*. **2010**, *353*, 77.
44. Aiello, D.; Mirabelli, I.; Testa, F.; *J. Sol-Gel Sci. Technol*. **2012**, *64*, 1.
45. Lai, S.-W.; Lin, H.-L.; Yu, T. L.; Lee, L.-P.; Weng, B.-J.; *Int. J. Hydrogen Energy* **2012**, *37*, I4393.

46. Marin-Astorga, N.; Martinez, J. J.; Borda, G.; Cubillos, J.; Suarez, D. N.; Rojas, H.; *Top. Catal*. **2012**, *55*, 620.
47. Yu, H.; Xue, X.; Huang, D.; *Mater. Res. Bull*. **2009**, *44*, 2112.
48. Yan, B.; Li, Y.; Zhou, B.; *Microporous Mesoporous Mater*. **2009**, *120*, 317.
49. Qiao, X.; Yan, B.; *J. Phys. Chem. B* **2008**, *112*, 14742.
50. Tang, A.; Deng, Y.; Jin, J.; Yang, H.; *Sci. World J*. **2012**, *2012*, 8.
51. Mirji, S. A.; Halligudi, S. B.; Sawant, D. P.; Jacob, N. E.; Patil, K. R.; Gaikward, A. D.; Pradhan, S. D.; *Appl. Surf. Sci*. **2006**, *252*, 4097.
52. Jabariyan, S.; Zanjanchi, M. A.; *Ultrason. Sonochem.* **2012**, *19*, 1087.
53. Rafatullah, M.; Sulaiman, O.; Hashim, R.; Ahmad, A.; *J. Hazard. Mater*. **2010**, *117*, 70.
54. Gong, Z.; Alef, K.; Wilke, B.-M.; Li, P.; *J. Hazard. Mater.* **2007**, *143*, 372.
55. Zeledón-Toruño, Z. C.; Lao-Luque, C.; De las Heras, F. X. C.; Sole-Sardans, M.; *Chemosphere* **2007**, *67*, 505.
56. Robinson, T.; Chandran, B.; Nigam, P.; *Bioresour. Technol*. **2002**, *85*, 119.
57. Ho, Y. S.; Mckay, G.; *Process Biochem. Res*. **1999**, *34*, 451.
58. Khattri, S. D.; Singh, M. K.; *Water, Air, Soil Pollut*. **2000**, *120*, 283.
59. Netpradit, S.; Thiravetyan, P.; Towprayoon, S.; *J. Colloid Interface Sci*. **2004**, *270*, 255.
60. Özcan, A. S.; Özcan, A.; *J. Colloid Interface Sci*. **2004**, *276*, 39.
61. Tang, H.; Zhou, W.; Zhang, L.; *J. Hazard. Mater*. **2012**, *209-210*, 218.
62. Ho, Y. S.; Mckay, G.; *Resour. Conserv. Recy*. **1999**, *25*, 171.
63. Özacar, M.; Sengil, I. A.; *Eng. Aspect*. **2004**, *242*, 105.
64. Romero-Gonzalez, J.; Peralta-Videa, J. R.; Rodrıguez, E.; Ramirez, S. L.; Gardea-Torresdey, J. L.; *J. Chem. Thermodyn*. **2005**, *37*, 343.
65. Parida, K. M.; Dash, S. K.; *J. Hazard. Mater*. **2010**, *179*, 642.
66. Santos, D. O.; Santos, M. L. N.; Costa, J. A. S.; De Jesus, R. A.; Navickiene, S.; Sussuchi, E. M.; De Mesquita, M. E.; *Environ Sci. Pollut Res*. **2013**, *20*, 5028.
67. Eftekhari, S.; Habibi-Yangjeh, A.; Sohrabnezhad, Sh.; *J. Hazard. Mater*. **2010**, *178*, 349.
68. Juang, L.-C.; Wang, C.-C.; Lee, C.-K.; *Chemosphere* **2006**, *64*, 1920.
69. Heidari, A.; Younesi, H.; Mehraban, Z.; *Chem. Eng. J*. **2009**, *153*, 70.
70. Araújo, R. S.; Azevedo, D. C. S.; Cavalcante Jr, C. L.; Jiménez-López, A.; Rodríguez-Castellón, E.; *Microporous Mesoporous Mater*. **2008**, *108*, 213.
71. Liu, Y.; Liu, Z.; Gao, J.; Dai, J.; Han, J.; Wang, Y.; Xie, J.; Yan, Y.; *J. Hazard. Mater*. **2011**, *186*, 197.

Submitted: April 14, 2013
Published online: December 3, 2013

FAPESP has sponsored the publication of this article.